International Journal of Applied Earth Observations and Geoinformation 103 (2021) 102464

Contents lists available at ScienceDirect

International Journal of Applied Earth Observations and Geoinformation

journal homepage: www.elsevier.com/locate/jag

Characterization of a seasonally snow-covered evergreen forest ecosystem

Qingyuan Zhang *

Cooperate Institute of Climate Science, Earth System Science Interdisciplinary Center, University of Maryland, College Park, MD 20740, United States
Center for Satellite Applications and Research, NESDIS, NOAA, College Park, MD 20740, United States

ARTICLE INFO

Keywords:
Evergreen forest
Snow
Boreal
LVS3
$fAPAR_{chl}$ and $fAPAR_{non\text{-}chl}$
GPP

ABSTRACT

It remains challenging to interpret seasonal profile of vegetation dynamics from empirical indices NDVI and EVI for boreal forests due to confounding impacts of snow, soil and snowmelt in winter and spring. This work aims to characterize the seasonally snow-covered Howland boreal forest ecosystem in Maine, USA with the Moderate Resolution Imaging Spectrometer (MODIS) images. Vegetation cover fraction (VGCF), fractional absorption of photosynthetically active radiation (fAPAR) by all canopy components ($fAPAR_{canopy}$), fAPAR by canopy chlorophyll ($fAPAR_{chl}$) and fAPAR by canopy non-chlorophyll components ($fAPAR_{non\text{-}chl}$) were extracted from MODIS images in multiple years (2001 - 2014). Snow exposed during December to April. Top of canopy viewable snow cover fraction in April of multiple years varied between 0.02 and 0.16 (0.06 ± 0.04). Seasonal VGCF and $fAPAR_{canopy}$ showed a summer plateau (VGCF: 0.97 ± 0.01; $fAPAR_{canopy}$: 0.90 ± 0.01). Both seasonal $fAPAR_{chl}$ and $fAPAR_{non\text{-}chl}$ changed with time, and seasonal $fAPAR_{non\text{-}chl}$ had a bimodal shape. Spring VGCF varied between 0.54 and 0.69 (0.61 ± 0.04). Spring $fAPAR_{chl}$ and $fAPAR_{non\text{-}chl}$ were 0.22 ± 0.03 and 0.21 ± 0.02, respectively. Peak summer $fAPAR_{chl}$ was 0.58 ± 0.02. The lowest summer $fAPAR_{non\text{-}chl}$ was 0.32 ± 0.02. Replacing $fAPAR_{canopy}$ with $fAPAR_{chl}$ to simulate boreal forest ecosystem gross primary production (GPP) could reduce uncertainties in GPP simulations.

1. Introduction

Satellite observations are valuable for providing global information of vegetative conditions and snow spatial–temporal extent (e.g., Gao et al., 2015; Moulin et al., 1997; Myneni et al., 2002; Running et al., 2004; Salomonson and Appel, 2004; Zhang et al., 2003) that is essential for carbon cycle studies, hydrological modeling, energy balance studies, climate modeling, water management, and agricultural management (e.g., Heinilä et al., 2019; Romanov et al., 2003; Peng et al., 2020). For instance, the normalized difference vegetation index (NDVI) (Rouse et al., 1974) and the enhanced vegetation index (EVI) (Huete et al., 2002) from the moderate resolution imaging spectrometer (MODIS) and other sensors have been often used for vegetation monitoring. Fractional absorption of photosynthetically active radiation (PAR) by the entire canopy ($fAPAR_{canopy}$), fractional absorption of PAR by canopy chlorophyll ($fAPAR_{chl}$), NDVI, and EVI have been utilized in estimation of ecosystem gross primary production (GPP) (e.g., Cheng et al., 2014; Xiao et al., 2004; Zhang et al., 2020). The normalized difference snow index (NDSI) from MODIS has been widely applied for snow monitoring (Hall et al., 2002).

During snow-free period, NDVI and EVI prove useful for mapping and monitoring forests. However, it remains challenging to interpret vegetation information from NDVI and EVI for forested areas during snow season. Forests bring difficulties to ground snow mapping (Klein et al., 1998) because forest cover obscures snow beneath the forest canopy while it contributes to the reflectance observed by a sensor (Romanov et al., 2003). Therefore, impacts of snow on NDVI and NDSI vary with forest cover (Hall et al., 2002; Lv and Pomeroy, 2019). NDVI (NDSI) values were positively (negatively) related with the forest cover fraction (Heinilä et al., 2014; Lv and Pomeroy, 2019).

Snowmelt is another extraneous factor affecting interpretation of these empirical indices for forested areas. Snowmelt increases soil moisture, and decreases surface reflectance. The reflectance reduction is greater in the water absorption bands around 1450 and 1950 nm. Snow and snowmelt bring challenges to vegetation monitoring with empirical vegetation indices (e.g., Moulin et al., 1997; Reed et al., 1994). Reed et al. (1994) reported that snow could reduce NDVI values of conifer forests, but snowmelt could increase NDVI values. In addition, snow and snowmelt also affect the index of near-infrared (NIR) reflectance of vegetation (NIR_v) (Badgley et al., 2017; Zeng et al., 2019), a product of

* Corresponding author. Address: 5825 University Research Court, College Park, MD 20740, United States.
E-mail addresses: qyzhang@umd.edu, qyz72@yahoo.com.

https://doi.org/10.1016/j.jag.2021.102464
Received 1 May 2021; Received in revised form 19 June 2021; Accepted 23 July 2021
Available online 26 August 2021

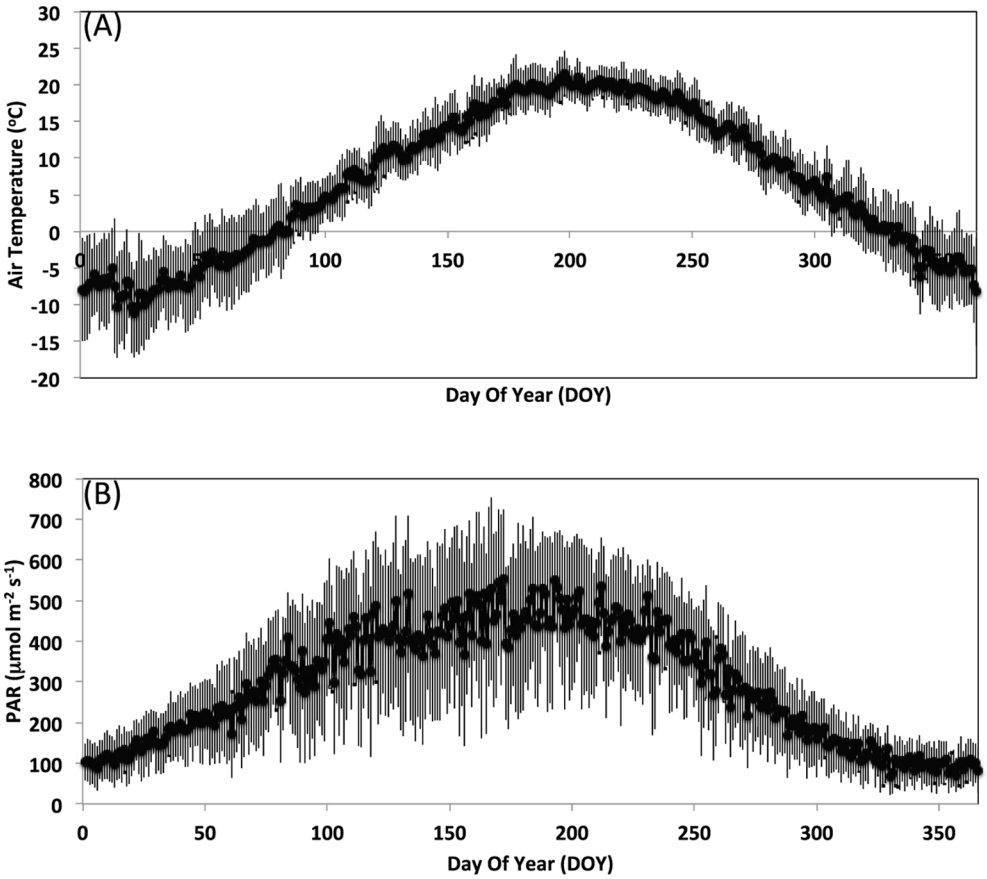

Fig. 1. (A) The 19-year-average daily air temperature (°C) for 1996 –2014; and (B) the 19-year-average daily photosynthetically active radiation (PAR) (mmol m^{-2} s^{-1}), bars are standard deviations.

Table 1
Spring (DOY 72–152) air temperature and PAR (high temperatures are highlighted).

Year	Air Temperature (°C)	PAR (μmol$m^{-2}s^{-1}$)
2001	6.4	406.5
2002	5.3	354.5
2003	4.7	341.7
2004	5.4	362.3
2005	5.2	346.7
2006	**7.5**	381.2
2007	5.1	370.1
2008	5.4	396.0
2009	6.5	377.6
2010	**9.1**	381.9
2011	6.5	362.9
2012	**7.7**	391.0
2013	6.2	400.6
2014	4.7	392.3

NDVI and reflectance of the NIR band.

Chapin et al. (2000) synthesized major North American high-latitude research programs and reported a positive correlation between NDVI of boreal forests and spring temperature. However, Goetz et al. (2005) analyzed NDVI of boreal forest areas and did not conform this positive correlation. Snow, snowmelt and soil can be confounding factors that affect interpretation of NDVI because they also contribute to reflectance of the two bands for NDVI computing. Zhang et al. (2020) presented the coupled Leaf-Vegetation-Soil-Snow-Surface water body (LVS3) radiative transfer model that fits the need in Arctic and boreal areas to retrieve information of vegetation and snow from optical sensors. The LVS3 model has been applied for the Utqiaġvik tundra ecosystem in Alaska to retrieve cover fractions of vegetation (VGCF), snow (SNOWCF), soil (SOILCF), and surface water bodies (WaterBodyCF), leaf area index (LAI), canopy chlorophyll content (CCC), foliar dry matter, $fAPAR_{chl}$, fractional absorption of PAR by canopy non-chlorophyll components ($fAPAR_{non\text{-}chl}$) and $fAPAR_{canopy}$. Absorption of PAR by canopy chlorophyll ($APAR_{chl}$) indicates potential photosynthetic capability and can be computed from $fAPAR_{chl}$ and climatic PAR data ($APAR_{chl} = fAPAR_{chl} \times PAR$).

The Howland boreal forest ecosystem in Maine has different characteristics from the Utqiaġvik tundra ecosystem. The tundra ecosystem is non-forested. VGCF value for the tundra ecosystem is very low in snow season. In contrast, the Howland boreal ecosystem contains certain conifer forest, and MODIS can't see snow/snowmelt beneath dense forest canopy. This study utilizes the LVS3 model for the boreal forest ecosystem to retrieve VGCF, SOILCF, SNOWCF, $fAPAR_{chl}$, $fAPAR_{non\text{-}chl}$, etc.

Previous investigations reported that correlation between net ecosystem exchange (NEE) and the length of carbon uptake period (CUP) for evergreen needleaf forests was strong (e.g., Churkina et al., 2005; Richardson et al., 2010). Hollinger et al. (2004) showed that springtime temperatures were significantly correlated with C uptake at the Howland forest. Richardson et al. (2009, 2010) expressed that the interannual variability in springtime temperatures explained a considerable proportion of the interannual variability in spring GPP for both conifer and broadleaved forests. The hypothesis is that higher spring temperature increases plant photosynthetic activity in terms of $APAR_{chl}$ at boreal forest ecosystems.

The objectives of this study are: [1] to characterize the boreal forest ecosystem with VGCF, $fAPAR_{canopy}$, $fAPAR_{chl}$ and $fAPAR_{non\text{-}chl}$; [2] to investigate when and how much snow over the Howland forest region

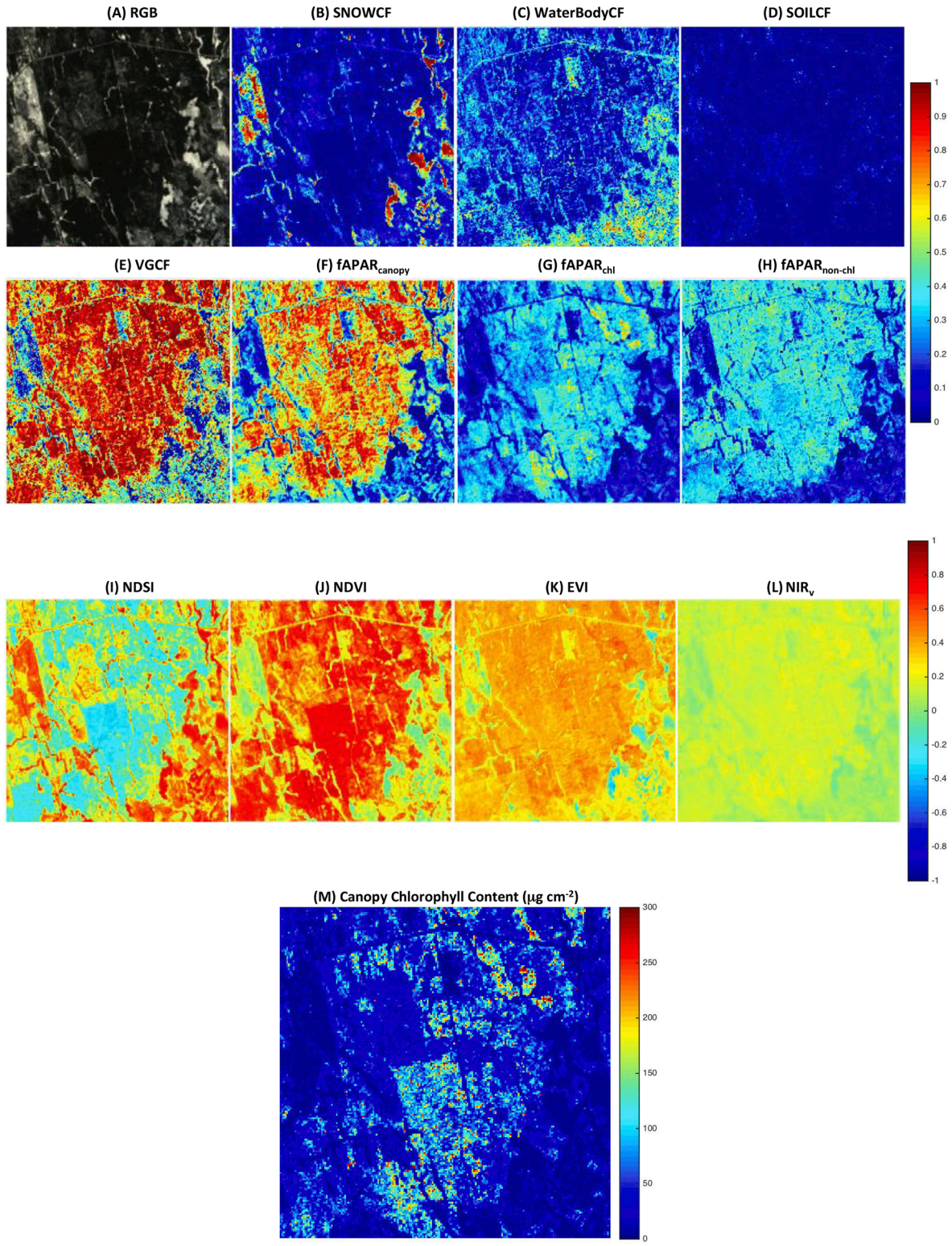

Fig. 2. The 6 × 6 km^2 Howland forest area in Maine: (A) the true color image obtained by the EO-1 Hyperion on March 5, 2014 (DOY 64) at a spatial resolution of 30 m; and maps of (B) snow cover fraction (SNOWCF); (C) surface water cover fraction (WaterBodyCF); (D)soil cover fraction (SOILCF); (E) vegetation cover fraction (VGCF); (F) fAPAR$_{canopy}$; (G) fAPAR$_{chl}$; (H) fAPAR$_{non-chl}$; (I) NDSI; (J) NDVI; (K) EVI; (L) NIR$_v$; and (M) canopy chlorophyll content (μg cm^{-2}), (B) – (H) share the upper legend describing values between 0 and 1, and (I) – (L) share the middle legend describing values between −1 and 1. Note that values of EVI less than −1 or greater than 1 are not shown.

exposes to MODIS in terms of SNOWCF, i.e., top of canopy snow cover fraction; [3] to investigate when and how much soil exposes to MODIS in terms of SOILCF; and [4] to investigate the hypothesis using climatic measurements in conjunction with MODIS fAPAR$_{chl}$ data.

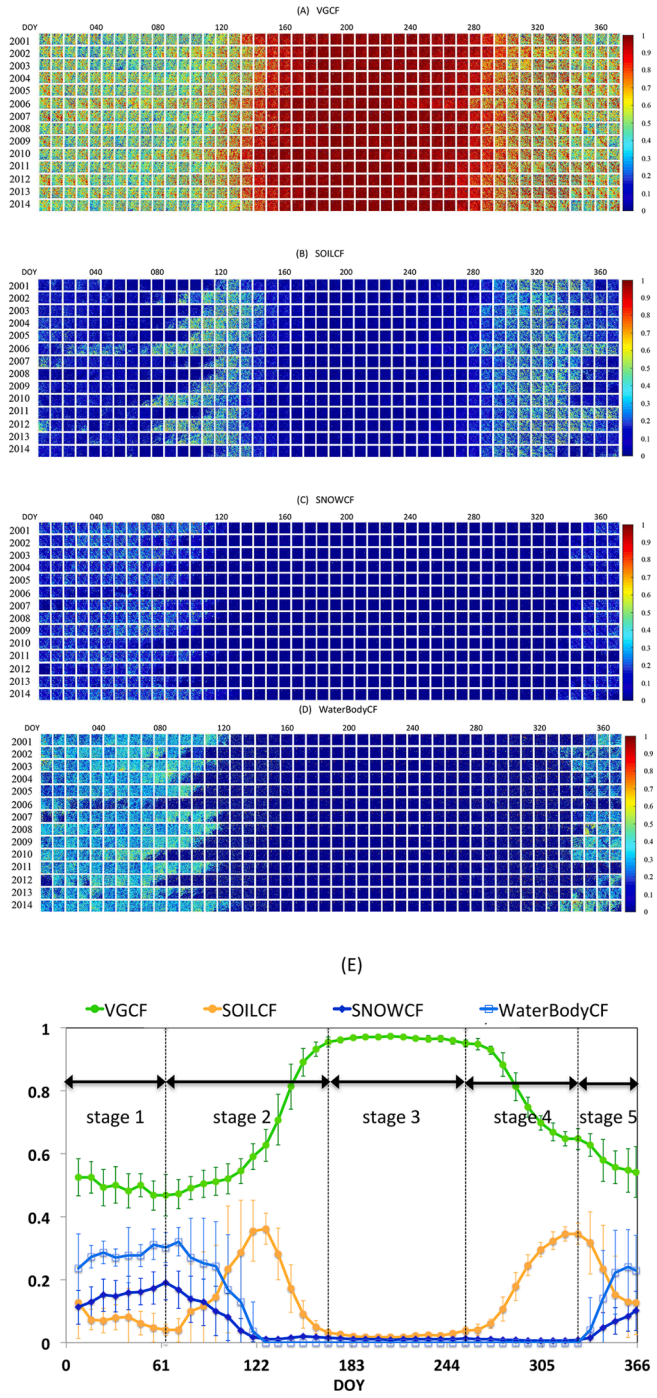

Fig. 3. MODIS 8-day seasonal dynamics of (A) VGCF; (B) SOILCF; (C) SNOWCF and (D) WaterBodyCF during 2001–2014, and (E) the 14-year average seasonal 8-day VGCF, SOLCF, SNOWCF and WaterBodyCF for the 50 × 50 km^2 surrounding area of the US-Ho1 site, bars are standard deviations. Note that the water sub-model of LVS3 includes muddy soils/water.

2. Methods

2.1. Study area

The US-Ho1 site (location: 45.2041° N, 68.7402° W), part of the Ameriflux network (https://ameriflux.lbl.gov/sites/siteinfo/US-Ho1), is a mature temperate-boreal transitional forest at Howland in Maine. Micrometeorology measurements include climatic PAR, air temperature, wind speed and precipitation since 1996. The vegetation around the US-Ho1 site is mainly conifers and some hardwoods. The soils are glacial tills with low fertility and high organic composition (Hollinger et al., 1999). Summer LAI of this site is about 5.3 m^2/m^2 (Xiao et al., 2004). A 50 × 50 km^2 region centered at the US-Ho1 site was selected to study temporal dynamics of vegetation.

2.2. Satellite images and the inversion approach

Zhang et al. (2020) has detailed description of the way to process MODIS satellite data and spectrally MODIS-like data, and the LVS3 model. This paper provides major points. Fourteen-year MODIS data from Terra and Aqua (2001–2014) were atmospherically corrected with the multi-angle implementation of atmospheric correction (MAIAC) algorithm (https://modis-land.gsfc.nasa.gov/MAIAC.html) (Lyapustin et al., 2018) and were processed to 8-day composites for the 50 × 50 km^2 boreal forest study region, (Cheng et al., 2014; Zhang et al., 2014a,b, 2015, 2020). This study utilized surface reflectance (ρ) data of all seven "land" bands of cloud-free observations: visible (band 3, blue: 459–479 nm; band 4, green: 545–565 nm; band 1, red: 620–670 nm), near infrared (band 2, NIR_1: 841–875 nm; band 5, NIR_2: 1230–1250 nm), and shortwave infrared (band 6, $SWIR_1$: 1628–1652 nm; band 7, $SWIR_2$: 2105–2155 nm). The MODIS images were used as input for LVS3 retrievals, and were used to compute NDVI, EVI and NIR_v.

The Hyperion visible to shortwave infrared (VSWIR) spectrometer covers the spectral ranges of the MODIS bands 1–7 (Zhang et al., 2012, 2013, 2016, 2020). The Hyperion 30 m images overlapping this 50 × 50 km^2 study region surrounding the US-Ho1 site were limited, and they did not cover the entire region. Therefore, one cloud free and near nadir Hyperion image that covered the US-Ho1 site was acquired on day of year (DOY) 64 in 2014. A surrounding 6 × 6 km^2 area of the US-Ho1 site was subset from this Hyperion image for visual evaluation with fine spatial details.

An improved version of the leaf model PROSPECT (Baret and Fourty, 1997) with five variables is used in LVS3 to simulate leaf optical properties: leaf internal structure variable; leaf total chlorophyll content (C_{ab}); leaf dry matter content (C_m); leaf water thickness (C_w) and leaf brown pigment (C_{brown}) (Zhang et al., 2006, 2009; Zhang et al., 2005). The vegetation model SAIL (Verhoef, 1998) considers LAI, stem area index, stem fraction, VGCF, etc., and has been employed alone or coupled with PROSPECT to simulate optical properties of vegetation (e.g., Jacquemoud et al., 2009; Yang et al., 2020b; Zhang et al., 2012). The SAIL model is used in LVS3 to simulate canopy optical properties. (Zhang et al., 2009, 2012, 2013, 2014a, 2015, 2016) successfully developed a two-variable model to mimic soil: soil cover fraction (SOILCF), and soil profile variable ($SOIL_A$). Similarly, snow and surface water bodies in the LVS3 model are simulated with two snow variables and two water body variables, respectively (Zhang et al., 2020).

The Metropolis algorithm (Zhang et al., 2006; Zhang et al., 2005), a type of Markov Chain Monte Carlo (MCMC) estimation procedure, is employed to invert the LVS3 model. The Metropolis algorithm estimates posterior probability distributions of the variables of LVS3 by inspection of the retrieved distributions, e.g., VGCF, SNOWCF, SOILCF, WaterBodyCF, C_{ab}, LAI, etc. From the posterior distributions of the variables, one then obtains the solutions of CCC, foliar dry matter, $fAPAR_{canopy}$, $fAPAR_{chl}$ and $fAPAR_{non\text{-}chl}$, etc. with LVS3.

3. Results

3.1. Climate

The US-Ho1 research site is among the pioneering AmeriFlux tower sites. I analyzed the micrometeorology data of this site from 1996 to 2014. This site had a mean annual precipitation of 857.8 mm. It had a mean annual wind speed of 2.6 m s^{-1} and mean annual temperature of 6.8 °C, with a minimum mean monthly temperature of –8.1 °C in January and a maximum mean monthly temperature of 19.9 °C in July.

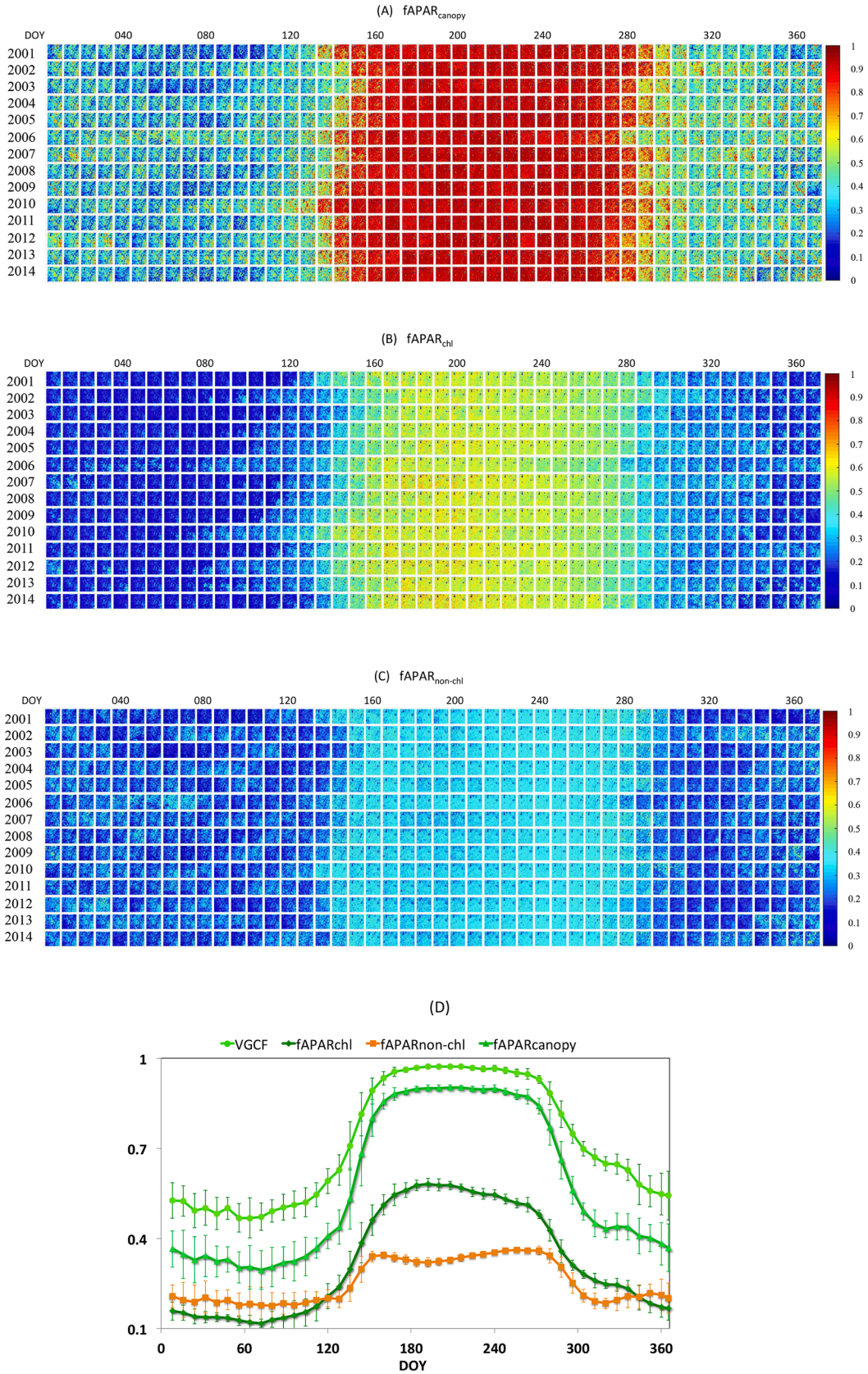

Fig. 4. MODIS 8-day seasonal dynamics of vegetation: (A) fAPAR$_{canopy}$; (B) fAPAR$_{chl}$; and (C) fAPAR$_{non-chl}$ during 2001–2014, and (DD) the 14-year average seasonal 8-day VGCF, fAPAR$_{canopy}$, fAPAR$_{chl}$ and fAPAR$_{non-chl}$ for the 50 × 50 km^2 block surrounding the US-Ho1 site, bars are standard deviations.

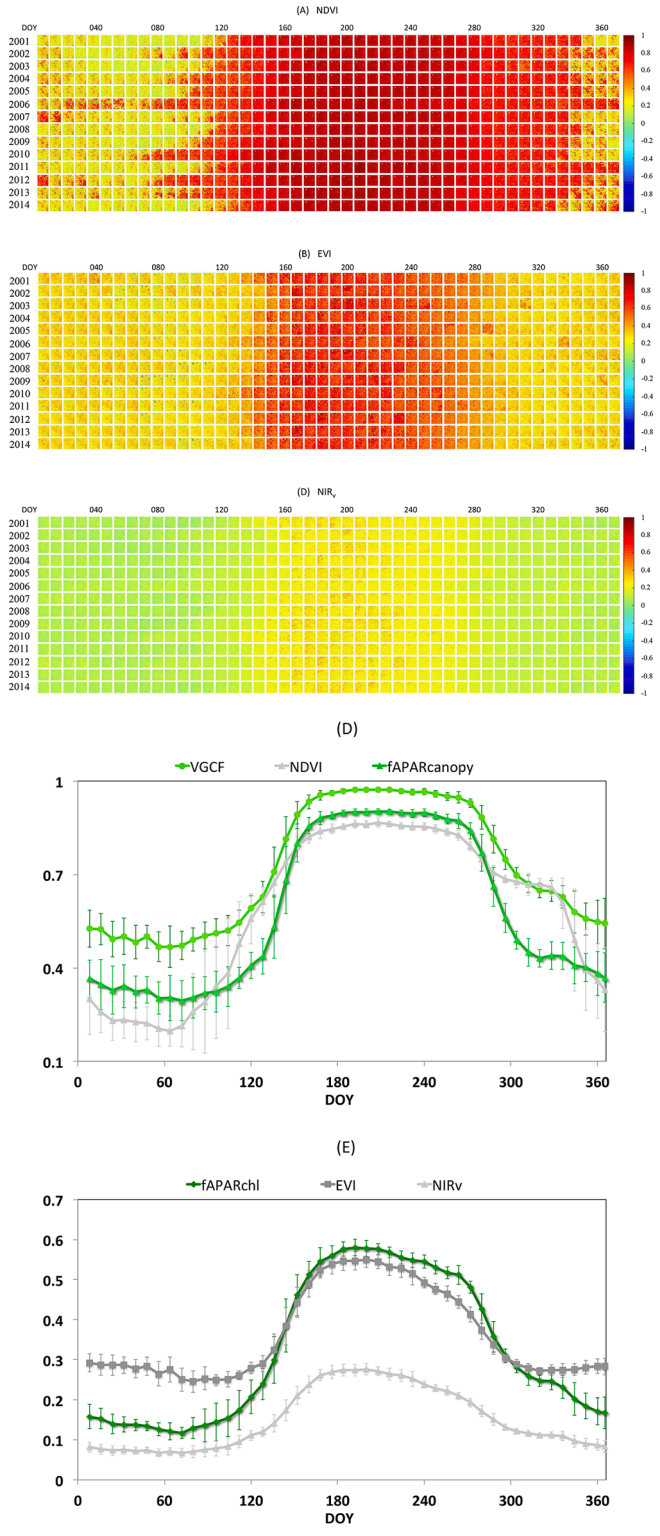

Fig. 5. MODIS 8-day seasonal dynamics of : (A) NDVI; (B) EVI; and (C) NIR_v during 2001–2014, (D) the 14-year average seasonal 8-day VGCF, NDVI and $fAPAR_{canopy}$, and (E) the 14-year average seasonal 8-day $fAPAR_{chl}$, EVI, and NIR_v for the 50 × 50 km^2 surrounding area of the US-Ho1 site, bars are standard deviations.

Temperature, soil moisture and climatic PAR are among the factors of vegetation growth and photosynthetic phenology. Snow, snowmelt and precipitation have impacts on temperature and soil moisture. The multiyear-average daily air temperature increased from spring to late June, remained relatively stable until August, and declined afterward toward winter (Fig. 1 A). On average, air temperature was above 0 °C during day of year (DOY) 80–331 and below 0 °C between DOY 332 and the following DOY 79. Spring (DOY 72–152) average temperature was ≥ 7.5 °C in 2006, 2010 and 2012 while ≤ 6.5 °C in other years during 2001–2014 (Table 1). The multiyear-average daily PAR increased from spring to summer (DOY 160–248), was very variable in the spring and summer, and declined in fall (DOY 256–328) (Fig. 1 B). Multiyear average seasonal values of PAR (1996–2014) were 373.0, 452.4, 219.9 and 140.0 $\mu molm^{-2}s^{-1}$ in spring, summer, fall and winter, respectively. Thus, PAR values in these seasons were 31%, 38%, 19% and 12% of the value of annual total PAR, respectively. Spring PAR in 2001–2014 was also listed in Table 1.

3.2. *Visual evaluation of LVS3 retrievals with fine spatial details using one Hyperion image*

Snow and snowmelt often present at Howland forest in the winter-spring snow season. Retrievals from the LVS3 model with the Hyperion 30 m image on DOY 64, 2014 can be visualized with fine spatial details of the surrounding 6 × 6 km^2 area of the US-Ho1 site. Open and sparsely forested areas with large snow cover viewable by the sensor were identified, and the extremely dense forest areas had limited snow cover viewable by the sensor (Fig. 2 A and 2 B). Open water contained in wetlands, small lakes and ponds and viewable snowmelt, or shadows were determined (Fig. 2 C). There was little bare soil ground viewable by the sensor on the collecting day (Fig. 2 D). Fig. 2B–2E maps SNOWCF, WaterBodyCF, SOILCF and VGCF, with mean values of 0.08, 0.17, 0.02, and 0.72, respectively. Fig. 2F–2H maps $fAPAR_{canopy}$, $fAPAR_{chl}$ and $fAPAR_{non\text{-}chl}$, with mean values of 0.57, 0.25 and 0.32, respectively. Fig. 2I–2L manifests NDSI, NDVI, EVI and NIR_v, with values of 0.27, 0.36, 0.32 and 0.11, respectively. Fig. 2 M maps CCC-, with mean value of 31.42 μg cm^{-2}. Densely forested areas had high values of VGCF, CCC, $fAPAR_{canopy}$ and $fAPAR_{chl}$, and low values of SNOWCF and NDSI, while open areas and wetlands had high values of NDSI, and low values of VGCF, CCC, $fAPAR_{canopy}$ and $fAPAR_{chl}$. There were differences between the widely used NDVI and $fAPAR_{chl}$. -

3.3. *Dynamics of cover fractions of vegetation, soil, snow and surface water*

Cover fractions of vegetation, soil, snow and surface water (VGCF, SOILCF, SNOWCF and WaterBodyCF) range between 0 and 1. Their temporal dynamics of the 50 × 50 km^2 block for 2001–2014 are displayed in Fig. 3. Each row in Fig. 3A–3D expresses values throughout a year with an interval of 8-day. High spring temperature in 2006, 2010 and 2012 (Table 1) was associated with low values of SNOWCF during DOY 88–112 of these three years. High spring temperature in these three years also resulted in earlier dates of spring peak for SOILCF. Fig. 3 E displays time series of the 14-year average seasonal VGCF, SOILCF, SNOWCF and WaterBodyCF with standard deviations. Snow exposed during December to April. There is terrain shadow at this time due to sun angle. Muddy soil and snowmelt has been modeled in the Surface water sub-model of the LVS3 model. Snow may melt after snow lands on the ground in winter and early spring. Terrain shadow has similar reflectance profile as water/snowmelt at MODIS bands. Therefore terrain shadow is nominally counted as "WaterBodyCF" for the first order analysis. If a lake or pond is covered by snow, LVS3 will recognize it as snow-covered. Soil exposed mostly in April, May, October and November.

Five phenological stages of vegetation growth and development were observed during a calendar year: [1] before green-up, snow, snowmelt and/or soil were exposed; [2] spring budding and green-up, VGCF increased rapidly with time prior to bloom; [3] summer bloom and pollination, VGCF reached a plateau once vegetative cover was complete, and remained during bloom until senescence began; [4] fall

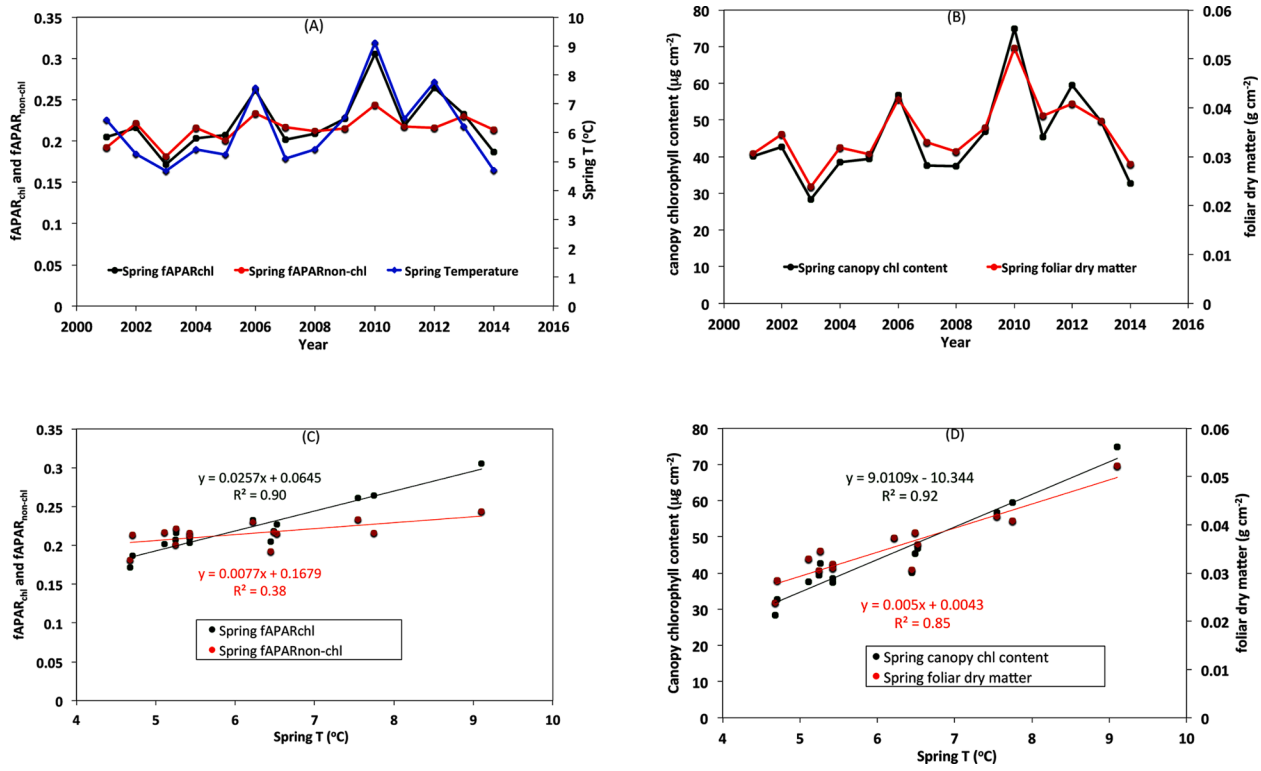

Fig. 6. (A) Time series of spring temperature, spring fAPAR$_{chl}$ and fAPAR$_{non-chl}$ for the 50 × 50 km^2 surrounding area of the US-Ho1 site in 2001–2014; (B) time series of spring canopy chlorophyll content (mg cm^{-2}) and foliar dry matter (g cm^{-2}) for the 50 × 50 km^2 surrounding area of the US-Ho1 site; (C) relationships between spring temperature and fAPAR$_{chl}$ and fAPAR$_{non-chl}$; and (D) relationships between spring temperature and canopy chlorophyll content and foliar dry matter.

senescence, deciduous leaves became chlorotic and started to lose from plants, and needle leaves became less green; and [5] after senescence, all deciduous leaves lost, more soil exposed, preparation for winter and snow, and VGCF resembled that measured at the first stage. It is worthy to note that the "after senescence" in one calendar year and the "before green-up" in the following calendar year can be combined into one stage from the perspective of surface dynamics of vegetation growth (Gao and Zhang, 2021; Zhang et al., 2018).

Fig. 3 E averages the five phenological stages in 2001–2014: the first stage (beginning of the year – DOY 064), the second stage (DOYs 072 – 152), the third stage (DOYs 160–248), the fourth stage (DOYs 256–328), and the fifth stage (DOYs 336 – end of the year). Interannual variations of VGCF, SOILCF, SNOWCF and WaterBodyCF were obvious in the first, second, and fifth stages. Minimal value for the 14-year average seasonal VGCF (0.47 ± 0.05) occurred on DOYs 56 – 72. Peak value for the 14-year average seasonal SNOWCF (0.19 ± 0.05) occurred on DOY 64. The seasonal SOILCF shows a double-peak shape due to snow and vegetation growth and development. Spring regional peak of SOILCF (0.36 ± 0.05) occurred on DOY 128 and late fall/early winter regional peak of SOILCF (0.35 ± 0.03) occurred on DOY 328. Spring seasonal VGCF varied between 0.54 and 0.69 (0.61 ± 0.04). Monthly SNOWCF in April varied between 0.02 and 0.16 (0.06 ± 0.04).

3.4. Dynamics of vegetation fAPAR$_{canopy}$, fAPAR$_{chl}$ and fAPAR$_{non-chl}$

Temporal dynamics of the three quantitative vegetation fAPAR variables (fAPAR$_{canopy}$, fAPAR$_{chl}$, and fAPAR$_{non-chl}$) are displayed in Fig. 4 with a range between 0 and 1. Each row in Fig. 4A–4C expresses values throughout a year with an interval of 8-day during 2001–2014. Fig. 4 D displays time series of the 14-year average seasonal VGCF, fAPAR$_{canopy}$, fAPAR$_{chl}$, and fAPAR$_{non-chl}$ with standard deviations.

During the third phenological stage in summer, both chlorophyll and non-chlorophyll components (fAPAR$_{chl}$ and fAPAR$_{non-chl}$) significantly contributed to fAPAR$_{canopy}$. Seasonal fAPAR$_{non-chl}$ had a bimodal shape. The first peak of fAPAR$_{non-chl}$ occurred after the spring peak of SOILCF, and the second peak of fAPAR$_{non-chl}$ occurred before the fall/winter peak of SOILCF. On DOY 64 (the day with peak SNOWCF value), 14-year average regional fAPAR$_{canopy}$, fAPAR$_{chl}$, and fAPAR$_{non-chl}$ were 0.30 ± 0.07, 0.12 ± 0.02, 0.18 ± 0.06, respectively. Peak average fAPAR$_{chl}$ occurred on DOY 192 (0.58 ± 0.02). The lowest average fAPAR$_{non-chl}$ in summer occurred on DOY 184 (0.32 ± 0.02). Spring fAPAR$_{chl}$ and fAPAR$_{non-chl}$ were 0.22 ± 0.03 and 0.21 ± 0.02, respectively.

3.5. Dynamics of NDVI, EVI and NIR$_v$

Temporal dynamics of the three vegetation indices (NDVI, EVI, and NIR$_v$) are displayed in Fig. 5 with a range between −1 and 1. Each row in Fig. 5 A–5C expresses values throughout a year from 2001 to 2014 with an interval of 8-day. Fig. 5D–5E displays time series of the 14-year average seasonal VGCF, fAPAR$_{canopy}$, NDVI, fAPAR$_{chl}$, EVI and NIR$_v$ with standard deviations. fAPAR$_{canopy}$, NDVI, fAPAR$_{chl}$ and EVI increased rapidly with time and with VGCF during the second phenological stage for green-up. Values of SOILCF in early 2006, 2007 and 2012 were greater than other years due to less SNOWCF and snowmelt (therefore WaterBodyCF) in those years,

The curves for 14-year average VGCF, fAPAR$_{canopy}$ and NDVI showed a plateau during the third stage in summer. The VGCF attained the highest summer estimates (0.97–0.98) among the four biophysical variables (VGCF, fAPAR$_{canopy}$, fAPAR$_{chl}$ and fAPAR$_{non-chl}$) and the three empirical indices (NDVI, EVI and NIR$_v$). The summer fAPAR$_{canopy}$ variable attained lower values than VGCF, ranging between 0.90 and 0.92. Annual peak values of NDVI were between 0.86 and 0.91, lower than VGCF and fAPAR$_{canopy}$. The dynamics of VGCF, fAPAR$_{canopy}$ and NDVI indicate that empirical VGCF–fAPAR$_{canopy}$–NDVI relationships may work reasonably well in summer for the Howland boreal forest ecosystem.

Temporal dynamics of fAPAR$_{chl}$ and EVI differ substantially from VGCF, fAPAR$_{canopy}$ and NDVI in terms of phase and magnitude. In

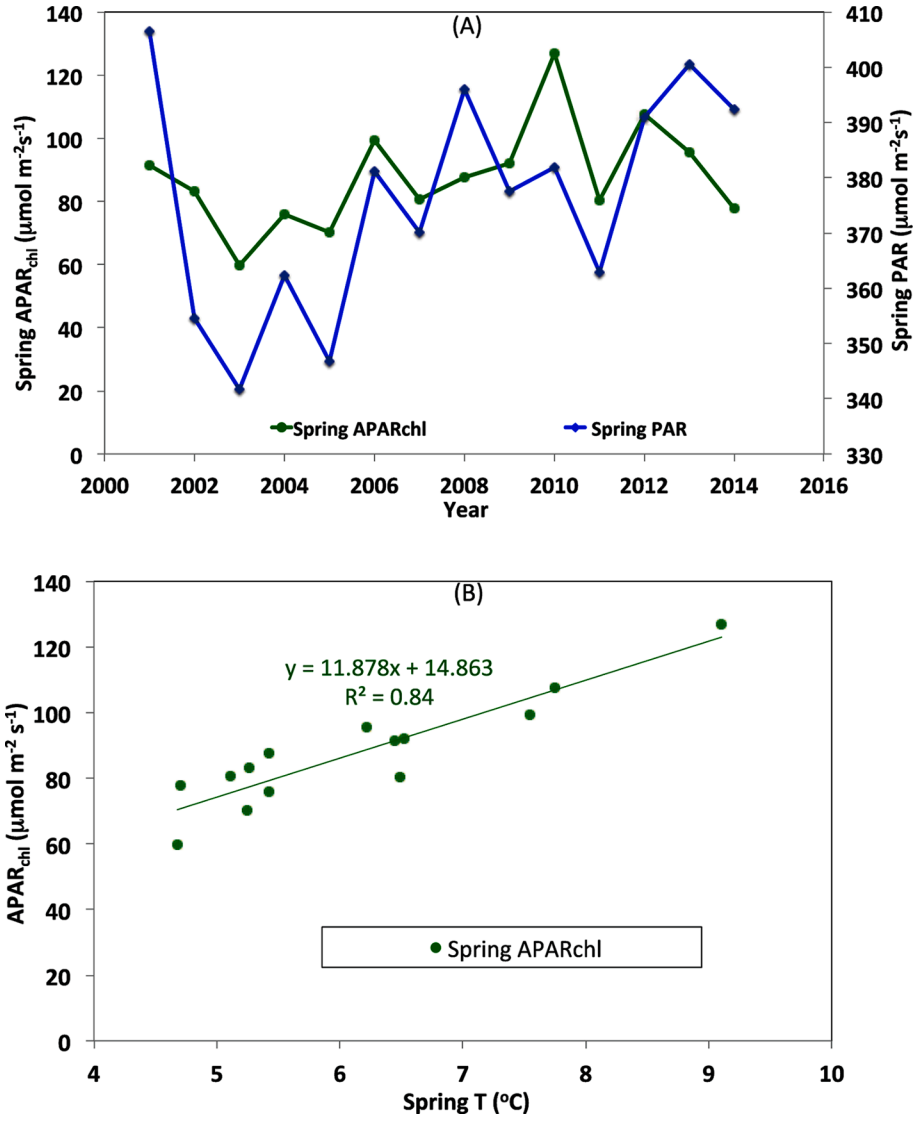

Fig. 7. (A) Time series of spring PAR and $APAR_{chl}$ for the 50 × 50 km^2 surrounding area of the US-Ho1 site in 2001–2014; and (B) relationship between spring temperature and spring $APAR_{chl}$.

contrast to the plateau of the curves for 14-year average VGCF, $fAPAR_{canopy}$ and NDVI in the summer, $fAPAR_{chl}$ and EVI changed with time in summer, reaching their peaks in early summer and then declining gradually. The temporal dynamics of EVI in the second, third and fourth stages from green-up to senescence is closely correlated to the dynamics of $fAPAR_{chl}$. The maximum values for $fAPAR_{chl}$ (0.58 ± 0.02) and EVI (0.55 ± 0.02) were much lower than VGCF, $fAPAR_{canopy}$ and NDVI.

The increase rate of NDVI in early spring was greater than those of both $fAPAR_{chl}$ and $fAPAR_{non\text{-}chl}$ (Fig. 4 D and 5 D), suggesting that other effects, such as changes in seasonal snow, snowmelt, soil, may be important factors affecting early spring NDVI, corresponding to previous studies, e.g., Moulin et al. (1997).

NIR_v attained the lowest summer estimates (0.28 ± 0.01) among the four biophysical variables and the three empirical indices. NDVI for the Howland boreal forest ecosystem saturated in summer while EVI and NIR_v did not appear to be saturated. As a result, EVI and NIR_v were still sensitive to phenological changes at leaf and canopy levels including the aging process of the leaves.

3.6. Impacts of springtime temperature on photosynthetic activity in spring

Previous studies investigated relationship between spring temperature and boreal forest growth, e.g., Richardson et al. (2009). Spring temperature of the Howland forest region in 2001–2014 was between 4.7 °C (in 2014) and 9.1 °C (in 2010) (Table 1 and Fig. 6 A). The three highest spring temperatures occurred in 2006 (7.5 °C), 2010 (9.1 °C) and 2012 (7.7 °C). Therefore, the spring snow-off dates in these three years were the earliest (Fig. 3 C). Warming means that more days are available for carbon assimilation and biomass growth. The greatest spring values of $fAPAR_{chl}$, $fAPAR_{non\text{-}chl}$, canopy chlorophyll content (CCC, unit: µg cm^{-2}) and foliar dry matter (unit: g cm^{-2}) in 2001–2014 occurred in 2010, and the lowest values occurred in 2003. Interannual spring bio-variability during 2001–2014 was large: $fAPAR_{chl}$ (0.17 to 0.31), $fAPAR_{non\text{-}chl}$ (0.18 to 0.24), CCC (28.39 to 74.83 µg cm^{-2}), and foliar dry matter (0.0238 to 0.0522 g cm^{-2}) (Fig. 6 A and 6B). Highly positive correlations between spring temperature and spring $fAPAR_{chl}$, CCC and foliar dry matter were identified, and $R^2 = 0.90$, 0.92 and 0.85, respectively. Statistics between spring temperature and spring $fAPAR_{non\text{-}chl}$ were $R^2 = 0.38$, $p = 0.018 < 0.05$ (Fig. 6C and 6D). Forest GPP is a function of $APAR_{chl}$ (GPP = $APAR_{chl}$ × ε, ε is light use efficiency).

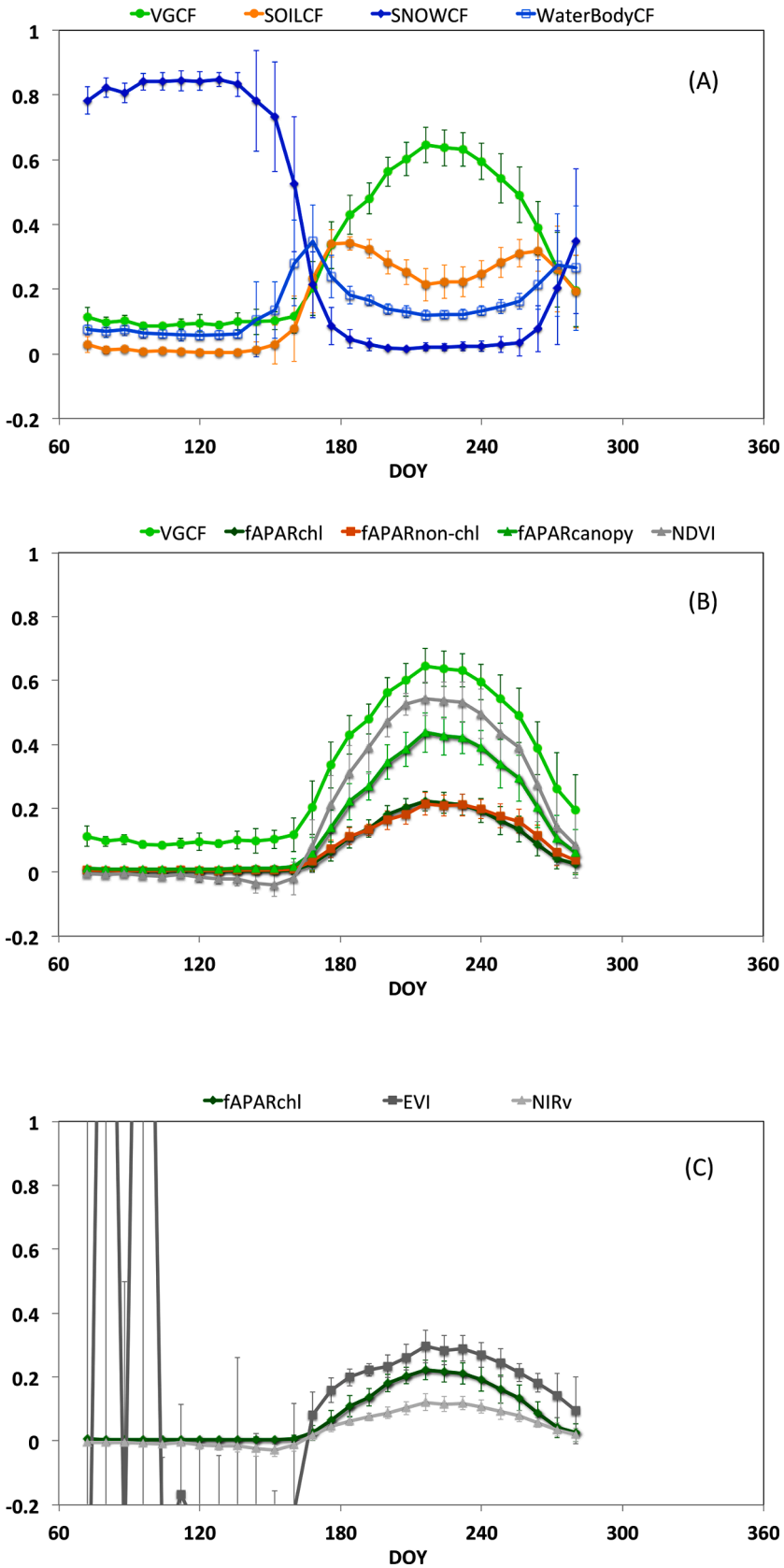

Fig. 8. (A) The 14-year-average seasonal 8-day VGCF, SOILCF, SNOWCF and WaterBodyCF for the 50 × 50 km^2 surrounding area of the US-Brw site in 2001–2014, (B) the 14-year-average seasonal 8-day VGCF, $fAPAR_{canopy}$, $fAPAR_{chl}$, $fAPAR_{non\text{-}chl}$ and NDVI, and (C) the 14-year-average seasonal 8-day $fAPAR_{chl}$, EVI and NIR_V, bars are standard deviations.

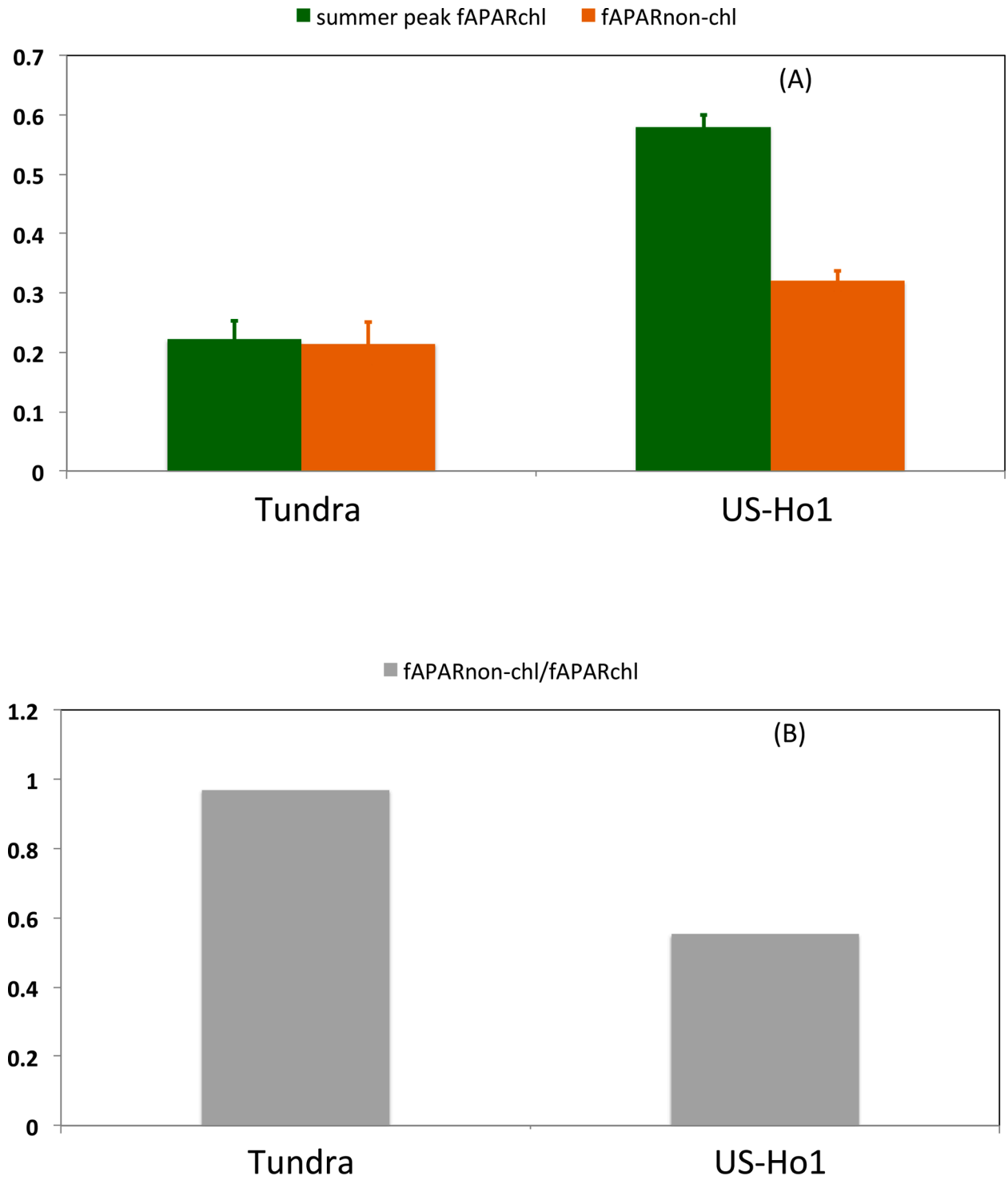

Fig. 9. Comparison of the 50 × 50 km^2 area of the Utqiaġvik tundra ecosystem in 2001–2014 and the 50 × 50 km^2 surrounding area of the US-Ho1 site in 2001–2014: (A) the peak value of the 14-year-average seasonal 8-day $fAPAR_{chl}$ for the tundra region and relative $fAPAR_{non\text{-}chl}$ versus those for the US-Ho1 region, and (B) the ratio of $fAPAR_{non\text{-}chl}$ over $fAPAR_{chl}$ for the tundra region versus the ratio for the US-Ho1 region, bars are standard deviations.

Interannual spring variability of PAR and $APAR_{chl}$ in 2001–2014 was large: PAR (341.68 μmol $m^{-2}s^{-1}$ in 2003 – 406.47 μmol $m^{-2}s^{-1}$ in 2001) and $APAR_{chl}$ (59.66 μmol $m^{-2}s^{-1}$ in 2003 – 127.06 μmol $m^{-2}s^{-1}$ in 2010) (Fig. 7 A). Highly positive correlation between spring temperature and spring $APAR_{chl}$ was found, and $R^2 = 0.84$ (Fig. 7 B). These findings support the hypothesis that higher spring temperature increases boreal forest $APAR_{chl}$.

4. Discussion

Tundra and evergreen needleleaf forest are two of the major plant functional types in the Arctic-boreal region. Zhang et al. (2020) studied the Utqiaġvik tundra ecosystem in Alaska with MODIS data (2001–2014). Fig. 8 exhibits -the 14-year average seasonal VGCF, SOILCF, SNOWCF, WaterBodyCF, $fAPAR_{canopy}$, $fAPAR_{chl}$, $fAPAR_{non\text{-}chl}$, NDVI, EVI and NIR_v with standard deviations. For observations in this

tundra area with high SNOWCF, values of EVI could be greater than 1 (Fig. 8 C). The Howland boreal forest ecosystem is different from the Utqiaġvik tundra ecosystem in terms of seasonal profiles of vegetation, snow, and soil. The Utqiaġvik tundra ecosystem has a high snow exposure in snow season while the Howland forest ecosystem does not have (Fig. 3 E and 8 A). As such, values for SNOWCF of the tundra ecosystem in snow season are greater than the boreal forest ecosystem. Fig. 4 A ($fAPAR_{canopy}$) indicates the standing boreal forests in snow season while Fig. 8 B ($fAPAR_{canopy}$) hints little standing vegetation of the tundra ecosystem in snow season (low stature/sparse vegetation). Temporal length between the two SOILCF peaks for the forest ecosystem is greater than temporal length for the tundra ecosystem (Figs. 3E and 8A). Summer VGCF, $fAPAR_{canopy}$ and NDVI of the forest ecosystem (Fig. 5 D) has a plateau shpe while the tundra ecosystem does not have (Fig. 8 B). $fAPAR_{non\text{-}chl}$ of the forest ecosystem has a bimodal shape while $fAPAR_{non\text{-}chl}$ of the tundra ecosytem does not have (Figs. 4D and 8B). Summer peak $fAPAR_{chl}$ for the forest ecosystem is greater than the EVI while summer peak $fAPAR_{chl}$ for the tundra ecosystem is less than the EVI (Figs. 5 E, and 8C).

It is critical to accurately simulate the absorbed PAR for vegetation photosynthesis and GPP in the terrestrial ecosystem models and land surface models because errors in these simulations propagate through the models to introduce additional errors in simulated biomass and other fluxes. The sunlight absorbed by the canopy chlorophyll ($APAR_{chl}$) is associated with the photochemistry process (primary pathway), the fluorescence from PSII and PSI, the non-photochemical quenching (NPQ) from PSII, and metabolic heat dissipation (sensible heat) (Rascher et al., 2015; van der Tol et al., 2014, 2016; Yang et al., 2017; Rascher et al., 2009; Rossini et al., 2015). The sunlight absorbed by the entire canopy ($APAR_{canopy}$) is also partially allocated to non-chlorophyll components ($APAR_{non\text{-}chl}$) for other processes (Rossini et al., 2010; Yang et al., 2020a). Seasonal $fAPAR_{chl}$ and $fAPAR_{non\text{-}chl}$ show the energy allocation strategy of the canopy. Both summer peak $fAPAR_{chl}$ and relative $fAPAR_{non\text{-}chl}$ of the forest ecosystem are greater than the tundra ecosystem (Fig. 9 A). The ratio $fAPAR_{non\text{-}chl}/fAPAR_{chl}$ indicates overestimating level of $APAR_{chl}$ when using $fAPAR_{canopy}$ to estimate $APAR_{chl}$. The overestimating level for the tundra ecosystem in summer is higher than the forest ecosystem (Fig. 9 B).

The bimodal shape of $fAPAR_{non\text{-}chl}$ of the forest ecosystem points out that this forest ecosystem allocates most of absorbed sunlight to chlorophyll for the photochemistry process in early summer than in other time of plant growing season. Sharp increase in PAR over the forest ecosystem in spring results in sharp trends of $fAPAR_{chl}$. The sensitivity of $fAPAR_{canopy}$ of the forest ecosystem in spring depends on the timing of full foliage cover. Partitioning $fAPAR_{canopy}$ into $fAPAR_{chl}$ and $fAPAR_{non\text{-}chl}$ is valuable for accurate estimates of the escape ratio of near-infrared solar-induced chlorophyll fluorescence (Yang et al., 2019, 2020a; Yang and van der Tol, 2018; Zeng et al., 2019).

The PhenoCam network provides repeat digital RGB images for many sites spanning a wide range of plant functional types, ecoregions, and climate zones (Richardson et al., 2018). The US-Ho2 site (location: 45.2128° N, 68.7418° W), ~775 m apart from the US-Ho1 site, is setup to study regrowing from the clearcut in 1990. The cameras on the US-Ho1 and US-Ho2 towers are taller than the forests, so that the fields of view of the cameras are across the landscapes. The evergreen forest dominates the images from the US-Ho1 camera while mixed forest dominates the images from the US-Ho2 camera. The camera on US-Ho1 started on 1/1/2007 (https://phenocam.sr.unh.edu/webcam/sites/howland1/) while the camera on US-Ho2 started on 3/30/2008 (https://phenocam.sr.unh.edu/webcam/sites/howland2/). Both cameras can see snow on trees in snow season while the camera on US-Ho1 (US-Ho2) can't (can) see snow on the ground. The fields of view of the cameras are different from the field of view of MODIS. It is challenging to quantitatively compare the camera images from the towers and the MODIS images straightforward. The green chromatic coordinate (GCC) and vegetation contrast index (VCI) computed with the digital numbers of PhenoCam's Red, Green and Blue bands are often used to track vegetation phenology (Richardson et al., 2018; Zhang et al., 2018). MODIS also has Red, Green and Blue spectral bands. Time series of GCC and VCI from MODIS may also be used to track vegetation phenology with the same methods developed for PhenoCam's GCC and VCI. Studies of time series of MODIS's GCC and VCI and comparison with PhenoCam's GCC and VCI in the future will be valuable.

5. Conclusions

VGCF and SNOWCF of the Howland ecosystem document dynamics and seasonal profiles of vegetation cover and exposure of snow.

Seasonal $fAPAR_{canopy}$, $fAPAR_{chl}$ and $fAPAR_{non\text{-}chl}$ of the Howland ecosystem reveal the energy allocation strategy of the canopy, indicating $fAPAR_{non\text{-}chl}$ is critical and changes in summer. Overestimating level of $APAR_{chl}$ with $fAPAR_{canopy}$ during summer peak $fAPAR_{chl}$ time is 55% (Fig. 9 B), hinting potential of replacing $fAPAR_{canopy}$ with $fAPAR_{chl}$ to reduce uncertainty in GPP estimates (Yang et al., 2020a).

The LVS3 model may be useful for flood and inundation monitoring (FIM) with optical satellite data, e.g. MODIS, VIIRS, advanced baseline imager (ABI), and advanced himawari imager (AHI), since it can provide information of cover fraction of open water bodies. Further research is needed to exclude terrain shadows, muddy soils, etc. from persistent water bodies for FIM products.

CRediT authorship contribution statement

Qingyuan Zhang: Investigation, Conceptualization, Methodology.

Declaration of Competing Interest

The author declares that he has no known competing financial interests or personal relationships that could have appeared to influence the work reported in this paper.

Acknowledgments

This study was supported by NOAA grant NA19NES4320002 (Cooperative Institute for Satellite Earth System Studies - CISESS), and NOAA grant NA20OAR4600288 (PI: Q. Zhang) at the University of Maryland/ESSIC. NASA's two programs also funded this work: the Terrestrial Ecology Program (Grant # NNX12AJ51G, PI: Q. Zhang) and the Science of Terra and Aqua Program (Grant # NNX14AK50G, PI: Q. Zhang). Micrometeorology measurements of the US-Ho1 site were downloaded from https://ameriflux.lbl.gov/sites/siteinfo/US-Ho1 (PI of the tower is Dr. David Hollinger).

References

Badgley, G., Field, C., Berry, J., 2017. Canopy NIR reflectance index (NIRv) and GPP. Sci. Adv. 3, e1602244.

Baret, F., & Fourty, T. (1997). Radiometric estimates of nitrogen status in leaves and canopies. Chapter 12, pp. 201-227. Berlin: Springer.

Chapin, F.S., McGuire, D., Randerson, J., Sr., R.P., Baldocchi, D., Hobbie, S.E., Roulet, N., Eugster, W., Kasischke, E., Rastetter, E.B., Zimov, S.A., & Running, S. (2000). Arctic-boreal ecosystems of western NA as components of the climate system. Global Change Biology, 6 (Supplement 1), 211 – 223.

Cheng, Y.-B., Zhang, Q., Lyapustin, A., Wang, Y., Middleton, E.M., 2014. Impacts of LUE and fAPAR Parameterization on GPP Modeling. Agric. For. Meteorol. 189–190, 187–197.

Churkina, Galina, Schimel, David, Braswell, Bobby H., Xiao, Xiangming, 2005. Spatial analysis of growing season length control over net ecosystem exchange. Glob. Change Biol. 11 (10), 1777–1787.

Gao, F., Hilker, T., Zhu, X., Anderson, M., Masek, J., Wang, P., Yang, Y., 2015. Landsat and MODerate-resolution-Imaging-Spectrometer Data Fusion for Vegetation Monitoring. IEEE GRSM 3, 47–60.

Gao, Feng, Zhang, Xiaoyang, 2021. Mapping Crop Phenology in Near Real-Time Using Satellite Remote Sensing: Challenges and Opportunities. Journal of Remote Sensing 2021, 1–14.

Goetz, S.J., Bunn, A.G., Fiske, G.J., Houghton, R.A., 2005. Satellite-observed photosynthetic NDVI trends across boreal NA linked with climate and fire

disturbance. Proceedings of the National Academy of Sciences of the United States of America (PNAS USA) 102 (38), 13521–13525.
Hall, D.K., Riggs, G.A., Salomonson, V.V., DiGirolamo, N.E., Bayr, K.J., 2002. Moderate Resolution Imaging Spectroradiometer snow cover products. Remote Sens. Environ. 83 (1–2), 181–194.
Heinilä, Kirsikka, Salminen, Miia, Metsämäki, Sari, Pellikka, Petri, Koponen, Sampsa, Pulliainen, Jouni, 2019. Reflectance variation in boreal landscape during the snow melting period using airborne imaging spectroscopy. Int. J. Appl. Earth Obs. Geoinf. 76, 66–76.
Heinilä, Kirsikka, Salminen, Miia, Pulliainen, Jouni, Cohen, Juval, Metsämäki, Sari, Pellikka, Petri, 2014. The effect of boreal forest canopy to reflectance of snow covered terrain based on airborne imaging spectrometer observations. Int. J. Appl. Earth Obs. Geoinf. 27, 31–41.
Hollinger, D., Goltz, S., Davidson, E.A., Lee, J.T., Tu, Kevin, & Valentine, H.T. (1999). Seasonal patterns and environmental control of carbon dioxide and water vapour exchange in the Howland forest. Global Change Biology, 5, 891-902.
Hollinger, D. Y., Aber, J., et al. (2004) Spatial and temporal variability in forest-atmosphere CO2 exchange. Global Change Biology, 10, 1689 – 1706.
Huete, A., Didan, K., Miura, T., Rodriguez, E.P., Gao, X., & Ferreira, L.G. (2002). Overview of the radiometric and biophysical performance of the Moderate Resolution Imaging Spectroradiometer vegetation indices. Remote Sensing of Environment, 83, 195-213.
Jacquemoud, S., Verhoef, W., Baret, F., Bacour, C., Zarco-Tejada, P., Asner, G., François, C., Ustin, S., 2009. PROSPECT+SAIL models: A review of use for PROSAIL vegetation characterization. Remote Sens. Environ. 113 (Supplement 1), S56–S66.
Klein, A., Hall, D., Riggs, G., 1998. Improving snow-cover mapping in forests through the use of combination of a snow reflectance model and a GeoSAIL canopy reflectance model. Hydrol. Process. 12, 1723–1744.
Lv, Zhibang, Pomeroy, John W., 2019. Detecting intercepted snow on mountain needleleaf forest canopies using satellite remote sensing. Remote Sens. Environ. 231, 111222. https://doi.org/10.1016/j.rse.2019.111222.
Lyapustin, Alexei, Wang, Yujie, Korkin, Sergey, Huang, Dong, 2018. MODIS Collection 6 MAIAC Algorithm. Atmos. Meas. Tech. 11 (10), 5741–5765.
Moulin, S., Kergoat, L., Viovy, N., Dedieu, G., 1997. Global-scale assessment of vegetation phenology using the National Oceanic and Atmospheric Administration's Advanced Very High Resolution Radiometer measurements. J. Clim. 10 (6), 1154–1170.
Myneni, R.B., Hoffman, S., Knyazikhin, Y., Privette, J.L., Glassy, J., Tian, Y., Wang, Y., Song, X., Zhang, Y., Smith, G.R., Lotsch, A., Friedl, M., Morisette, J.T., Votava, P., Nemani, R.R., Running, S.W., 2002. Global products of LAI and fAPAR from year one of MODerate-resolution-Imaging-Spectrometer data. Remote Sens. Environ. 83, 214–231.
Peng, B., Guan, K., Zhou, W., Jiang, C., Frankenberg, C., Sun, Y., He, L., Köhler, P., 2020. Assessing the benefit of satellite-based Solar-Induced Chlorophyll Fluorescence in crop yield prediction. Int. J. Appl. Earth Obs. Geoinf. 90, 102126.
Rascher, U., Agati, G., Alonso, L., Cecchi, G., Champagne, S., Colombo, R., Damm, A., Daumard, F., de Miguel, E., Fernandez, G., Franch, B., Franke, J., Gerbig, C., Gioli, B., Gómez, J. A., Goulas, Y., Guanter, L., Gutiérrez-de-la-Cámara, Ó., Hamdi, K., Hostert, P., Jiménez, M., Kosvancova, M., Lognoli, D., Meroni, M., Miglietta, F., Moersch, A., Moreno, J., Moya, I., Neininger, B., Okujeni, A., Ounis, A., Palombi, L., Raimondi, V., Schickling, A., Sobrino, J. A., Stellmes, M., Toci, G., Toscano, P., Udelhoven, T., van der Linden, S., and Zaldei, A. (2009). CEFLES2: the remote sensing component to quantify photosynthetic efficiency from the leaf to the region by measuring SIF in the oxygen absorption bands, Biogeosciences, 6, 1181–1198.
Rascher, U., Alonso, L., Burkart, A., Cilia, C., Cogliati, S., Colombo, R., Damm, A., Drusch, M., Guanter, L., Hanus, J., et al., 2015. Sun-induced fluorescence – a new probe of photosynthesis: First maps from the imaging spectrometer HyPlant. Glob. Change Biol. 21, 4673–4684.
Reed, B.C., Brown, J.F., VanderZee, D., Loveland, T.R., Merchant, J.W., & Ohlen, D.O. (1994). Phenology from the National Oceanic and Atmospheric Administration's Advanced Very High Resolution Radiometer Imagery. Journal of Vegetation Science, 5, 703 – 714.
Richardson, A. D., Hollinger, D. Y., Dail, D. B., Lee, J. T., Munger, J. W. & O'Keefe, J. (2009) Influence of spring phenology on seasonal and annual carbon balance in two contrasting New England forests. Tree Physiology, 29, 321–331.
Richardson, Andrew D., Andy Black, T., Cias, Philippe, Delbart, Nicolas, Friedl, Mark A., Gobron, Nadine, Hollinger, David Y., Kutsch, Werner L., Longdoz, Bernard, Luyssaert, Sebastiaan, Migliavacca, Mirco, Montagnani, Leonardo, William Munger, J., Moors, Eddy, Piao, Shilong, Rebmann, Corinna, Reichstein, Markus, Saigusa, Nobuko, Tomelleri, Enrico, Vargas, Rodrigo, Varlagin, Andrej, 2010. Influence of spring and autumn phenological transitions on forest ecosystem productivity. *Philosophical Transactions* of the *Royal Society* B: Biological Sciences 365 (1555), 3227–3246.
Richardson, Andrew D., Hufkens, Koen, Milliman, Tom, Aubrecht, Donald M., Chen, Min, Gray, Josh M., Johnston, Miriam R., Keenan, Trevor F., Klosterman, Stephen T., Kosmala, Margaret, Melaas, Eli K., Friedl, Mark A., Frolking, Steve, 2018. Tracking vegetation phenology across diverse North American biomes using PhenoCam imagery. Sci. Data 5 (1). https://doi.org/10.1038/sdata.2018.28.
Romanov, P., Tarpley, D., Gutman, G., Carroll, T., 2003. Snow cover fraction over NA from GOES. J. Geophys. Res. 108, 8619.
Rossini, M., Meroni, M., Migliavacca, M., Manca, G., Cogliati, S., Busetto, L., Picchi, V., Cescatti, A., Seufert, G., Colombo, R., 2010. High-resolution field spectroscopy measurements for estimating GEP in a rice field. Agric. For. Meteorol. 150 (9), 1283–1296.
Rossini, M., Nedbal, L., Guanter, L., Ač, A., Alonso, L., Burkart, A., Cogliati, S., Colombo, R., Damm, A., Drusch, M., Hanus, J., Janoutova, R., Julitta, T., Kokkalis, P., Moreno, J., Novotny, J., Panigada, C., Pinto, F., Schickling, A., Schüttemeyer, D., Zemek, F., & Rascher, Uwe, (2015). Red and far-red SIF as a measure of plant photosynthesis. Geophysical Research Letters, 42 (6), 1632–1639.
Rouse, Jr., J. W.,R. H. Haas, J. A. Schell, D. W. Deering, & J. C. Harlan (1974). MONITORING THE VERNAL ADVANCEMENT AND RETROGRADATION (GREENWAVE EFFECT) OF NATURAL VEGETATION, Type II I Report for 09/1972-11/1974, https://ntrs.nasa.gov/api/citations/19750020419/downloads/19750020419.pdf.
Running, S., Nemani, R., Heinsch, F., Zhao, M., Reeves, M., Hashimoto, H. (2004). A continuous satellite-derived measure of global terrestrial primary production. BioScience, 54, 547-560.
Salomonson, V.V., Appel, I., 2004. FSC from MODerate-resolution-Imaging-Spectrometer using the NDSI. Remote Sens. Environ. 89, 351–360.
van der Tol, C., Berry, J., Campbell, P., Rascher, U., 2014. Models of fluorescence and photosynthesis for interpreting measurements of SIF. *JGR*. Biogeosciences 119 (12), 2312–2327.
van der Tol, C., Rossini, M., Cogliati, S., Verhoef, W., Colombo, R., Rascher, U., Mohammed, G., 2016. A model and measurement comparison of diurnal cycles of SIF of crops. Remote Sens. Environ. 186, 663–677.
Verhoef, W., 1998. In: Theory of radiative transfer models applied in optical remote sensing of vegetation canopies. Wageningen University, p. 310 p..
Xiao, X., Hollinger, D., Aber, J., Goltz, M., Davidson, E.A., Zhang, Q., Moore, B., 2004. VGT-based modeling of GPP in the Howland forest. Remote Sens. Environ. 89, 519–534.
Yang, P., Verhoef, W., van der Tol, C., 2017. The mSCOPE model: a simple adaptation to the SCOPE model to describe reflectance, fluorescence and photosynthesis of vertically heterogeneous canopies. Remote Sens. Environ. 201, 1–11.
Yang, P., van der Tol, C., 2018. Linking canopy scattering of far-red sun-induced chlorophyll fluorescence with reflectance. Remote Sens. Environ. 209, 456–467.
Yang, P., van der Tol, C., Verhoef, W., Damm, A., Schickling, A., Kraska, T., Muller, O., Rascher, U., 2019. Using reflectance to explain vegetation biochemical and structural effects on sun-induced chlorophyll fluorescence. Remote Sens. Environ. 231, 110996.
Yang, P., van der Tol, C., Campbell, P.K.E., Middleton, E.M., 2020a. Fluorescence Correction Vegetation Index (FCVI): A physically based reflectance index to separate physiological and non-physiological information in far-red sun-induced chlorophyll fluorescence. Remote Sens. Environ. 240, 111676.
Yang, P., van der Tol, C., Yin, T., Verhoef, W., 2020b. The SPART model: A soil-plant-atmosphere radiative transfer model for satellite measurements in the solar spectrum. Remote Sens. Environ. 247, 111870.
Zeng, Y., Badgley, G., Dechant, B., Ryu, Y., Chen, M., Berry, J., 2019. A practical approach for estimating the escape ratio of NIR SIF. Remote Sens. Environ. 232, 111209.
Zhang, X., Friedl, M., Schaaf, C., Strahler, A., Hodges, J., Gao, F., Reed, B., Huete, A., 2003. Monitoring phenology using MODerate-resolution-Imaging-Spectrometer data. Remote Sens. Environ. 84, 471–475.
Zhang, Xiaoyang, Jayavelu, Senthilnath, Liu, Lingling, Friedl, Mark A., Henebry, Geoffrey M., Liu, Yan, Schaaf, Crystal B., Richardson, Andrew D., Gray, Joshua, 2018. Evaluation of land surface phenology from VIIRS data using time series of PhenoCam imagery. Agric. For. Meteorol. 256-257, 137–149.
Zhang, Q., Cheng, Y.-B., Lyapustin, A., Wang, Y., Zhang, X., Suyker, A., Verma, S., Shuai, Y., Middleton, E., 2015. Estimation of crop gross primary production (GPP): II. Do the scaled vegetation indices improve performance? Agric. For. Meteorol. 200, 1–8.
Zhang, Q., Cheng, Y.-B., Lyapustin, A.I., Wang, Y., Gao, F., Suyker, A., Verma, S., Middleton, E.M., 2014a. Estimation of crop gross primary production (GPP): $fAPAR_{chl}$ versus MOD15A2 FPAR. Remote Sens. Environ. 153, 1–6.
Zhang, Q., Cheng, Y.-B., Lyapustin, A.I., Wang, Y., Xiao, X., Suyker, A., Verma, S., Tan, B., Middleton, E.M., 2014b. Estimation of crop gross primary production (GPP): I. Impact of MODIS observation footprint area and Impact of vegetation BRDF characteristics. Agric. For. Meteorol. 191, 51–63.
Zhang, Q., Middleton, E., Gao, B.-C., Cheng, Y.-B., 2012. Using EO-1 Hyperion to Simulate HyspIRI Products for a Coniferous Forest: the Fraction of PAR Absorbed by Chlorophyll ($fAPAR_{chl}$) and Leaf Water Content (LWC). IEEE Trans. Geosci. Remote Sens. 50, 1844–1852.
Zhang, Qingyuan, Middleton, Elizabeth M., Cheng, Yen-Ben, Huemmrich, K. Fred, Cook, Bruce D., Corp, Lawrence A., Kustas, William P., Russ, Andrew L., Prueger, John H., Yao, Tian, 2016. Integrating chlorophyll fAPAR and nadir photochemical reflectance index from EO-1/Hyperion to predict cornfield daily gross primary production. Remote Sens. Environ. 186, 311–321.
Zhang, Q., Middleton, E.M., Cheng, Y.-B., Landis, D.R., 2013. Variations of Foliage Chlorophyll fAPAR and Foliage Non-Chlorophyll fAPAR ($fAPAR_{chl}$, $fAPAR_{non\text{-}chl}$) at the Harvard Forest. IEEE J. Sel. Top. Appl. Earth Obs. Remote Sens. 6, 2254–2264.
Zhang, Q., Middleton, E.M., Margolis, H.A., Drolet, G.G., Barr, A.A., Black, T.A., 2009. Can a MODIS-derived estimate of the fraction of PAR absorbed by chlorophyll

($FAPAR_{chl}$) improve predictions of light-use efficiency and ecosystem photosynthesis for a boreal aspen forest? Remote Sens. Environ. 113, 880–888.

Zhang, Q., Xiao, X., Braswell, B., Linder, E., Ollinger, S., Smith, M.L., Jenkins, J.P., Baret, F., Richardson, A.D., Moore, B., Minocha, R., 2006. Characterization of seasonal variation of forest canopy in a temperate deciduous broadleaf forest, using daily MODIS data. Remote Sens. Environ. 105, 189–203.

Zhang, Q., Xiao, X.M., Braswell, B., Linder, E., Baret, F., & Moore, B. (2005). Estimating light absorption by chlorophyll, leaf and canopy in a deciduous broadleaf forest using MODIS data and a radiative transfer model. Remote Sensing of Environment, 99, 357-371.

Zhang, Q., Yao, T., Middleton, E., Huemmrich, K.F., Lyapustin, A., Wang, Y., 2020. Evaluating impacts of snow, surface water, soil and vegetation on empirical vegetation and snow indices for the Utqiaġvik tundra ecosystem in Alaska with the LVS3 model. Remote Sens. Environ. 240, 111677.